

A Recursive Born Approach to Nonlinear Inverse Scattering

Ulugbek S. Kamilov*, Dehong Liu, Hassan Mansour, and Petros T. Boufounos

March 15, 2016

Abstract

The Iterative Born Approximation (IBA) is a well-known method for describing waves scattered by semi-transparent objects. In this paper, we present a novel nonlinear inverse scattering method that combines IBA with an edge-preserving total variation (TV) regularizer. The proposed method is obtained by relating iterations of IBA to layers of a feedforward neural network and developing a corresponding error backpropagation algorithm for efficiently estimating the permittivity of the object. Simulations illustrate that, by accounting for multiple scattering, the method successfully recovers the permittivity distribution where the traditional linear inverse scattering fails.

1 Introduction

Knowledge of the spatial distribution of the permittivity within an object is important for many applications since it enables the visualization of the internal structure and physical properties of the object. Measurements of the permittivity are typically obtained by first illuminating the object with a known incident wave and recording the resulting scattered waves with sensors located outside the object. The spatial map of permittivity is reconstructed from the measurements, using computational inverse scattering methods that rely on physical models describing the object-wave interaction.

Traditional approaches to inverse scattering formulate the task as a linear inverse problem by establishing a linear relationship between the permittivity and the scattered wave. The linear model can be obtained by assuming a straight-ray propagation of waves [1], or by adopting more refined single-scattering models based on the first Born [2] or Rytov approximations [3]. Once linearized, the problem can be efficiently solved using the preferred regularized reconstruction methods, typically based on sparsity and iterative optimization [4–6].

Recent experimental results indicate that the resolution and quality of the reconstructed permittivity is improved when nonlinear physical models are used instead of traditional linear ones [7–10]. In particular, nonlinear physical models can account for multiple scattering and provide a more accurate interpretation of the measured data at the cost of increased computational complexity of the reconstruction.

In this paper, we develop a new computational imaging method to reconstruct the permittivity distribution of an object from transmitted or reflected waves. Our method is based on a nonlinear physical model that can account for multiple scattering in a computationally efficient way. Specifically, we propose to interpret the iterations of the iterative Born approximation (IBA) as layers of a feedforward neural network. This formulation leads to an efficient error backpropagation algorithm used to evaluate the gradient of the scattered field with respect to the permittivity, thus enabling the recovery of the latter from a set of measured scattered fields. The quality of the final estimate is further enhanced by regularizing the solution with an edge-preserving total variation (TV) penalty. Our simulations indicate that the proposed method accurately models scattering without prohibitive computational overhead, and successfully recovers the object where the traditional linear approaches fail.

*U. S. Kamilov (email: kamilov@merl.com), D. Liu (email: liudh@merl.com), H. Mansour (email: mansour@merl.com), and P. T. Boufounos (email: petrosb@merl.com) are with Mitsubishi Electric Research Laboratories (MERL), 201 Broadway, Cambridge, MA 02140, USA.

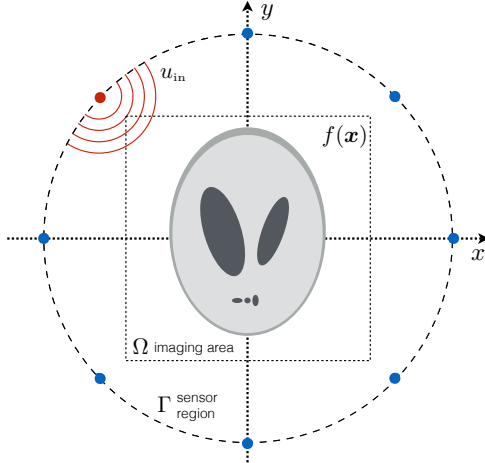


Figure 1: Schematic representation of a scattering scenario. An object with a scattering potential $f(\mathbf{x})$, $\mathbf{x} \in \Omega$, is illuminated with an input wave u_{in} , which interacts with the object and results in the scattered wave u_{sc} at the sensor region Γ . The scattered wave is measured and used to computationally form an image of f .

2 Related Work

A comprehensive review of nonlinear inverse scattering, with detailed description of standard algorithms, is available in the book-chapter by van den Berg [11].

Three common approaches to nonlinear inverse scattering are iterative Born [12–14], modified gradient [15–17], and contrast-source inversion methods [18]. All these methods attempt to iteratively minimize the discrepancy between the actual and predicted measurements, while enforcing the consistency of the fields inside the object. The actual optimization is performed in an alternating fashion by first updating the permittivity for a fixed field, and then updating the field for a fixed permittivity. The difference between the methods is in the actual computation of the updates.

Recently, the beam propagation method (BPM) was proposed for performing nonlinear inverse scattering in transmission [10, 19–21]. BPM-based methods circumvent the need to solve an explicit optimization problem for the internal field, by instead numerically propagating the field slice-by-slice through the object. It was shown that BPM can be related to a neural network where each layer corresponds to a spatial slice of the object. An efficient backpropagation algorithm can thus be derived to reconstruct the object from the measurements [21].

This paper substantially extends the BPM-based method by relying on IBA to formulate the nonlinear physical model. One main advantage of the proposed formulation over BPM is that it allows reconstruction when measuring reflections. Additionally, unlike alternating minimization schemes that assume a linear problem for a given internal field, our method directly optimizes the nonlinear model in a tractable way using error backpropagation.

3 Main Results

The method presented here can be generalized to a majority of tomographic experiments in transmission or reflection. For simplicity of derivations, we ignore absorption by assuming a real permittivity; however, the equations can be generalized to handle complex permittivities. We additionally assume coherent measurements, i.e., that both the amplitude and phase of the scattered wave are recorded at the sensor locations.

3.1 Problem Formulation

Consider the two-dimensional (2D) scattering problem illustrated in Fig. 1, where an object of real permittivity distribution $\epsilon(\mathbf{x})$, with $\mathbf{x} = (x, y) \in \Omega$, is immersed into the background medium of permittivity ϵ_b . The line sources that generate the electromagnetic excitation and the sensors collecting the data are located in the sensor region $\Gamma \subseteq \mathbb{R}^2$. By assuming, and ignoring, a time dependence $\exp(j\omega t)$, the incident electric field created by the ℓ th source, located at $\mathbf{x}_\ell \in \Gamma$, is given by

$$u_{\text{in}}(\mathbf{x}) = A \frac{j}{4} H_0^{(2)}(k_b \|\mathbf{x} - \mathbf{x}_\ell\|_{\ell_2}), \quad (1)$$

for all $\mathbf{x} \in \mathbb{R}^2$, where A is the strength of the source, $H_0^{(2)}$ is the zero-order Hankel function of the second kind, $k_b = k_0 \sqrt{\epsilon_b}$ is the wavenumber in the background medium, $k_0 = \omega/c_0 = 2\pi/\lambda$ is the wavenumber in free space, λ is the wavelength, and $c_0 \approx 3 \times 10^8$ m/s. In the subsequent derivations, we consider the scenario of a single illumination and drop the indices ℓ . The generalization to an arbitrary number of illuminations L is straightforward.

The Lippmann-Schwinger integral equation describes the relationship between the permittivity and the wave-field [11]

$$u(\mathbf{x}) = u_{\text{in}}(\mathbf{x}) + \int_{\Omega} g(\mathbf{x} - \mathbf{x}') f(\mathbf{x}') u(\mathbf{x}') d\mathbf{x}', \quad (2)$$

for all $\mathbf{x} \in \Omega$, where we define the *scattering potential*

$$f(\mathbf{x}) \triangleq k_b^2 (\epsilon_b - \epsilon(\mathbf{x})) \quad (3)$$

and the Green's function for the homogeneous medium

$$g(\mathbf{x}) \triangleq \frac{j}{4} H_0^{(2)}(k_b \|\mathbf{x}\|_{\ell_2}). \quad (4)$$

Similarly, the scattered field in the sensor region can be expressed as

$$u_{\text{sc}}(\mathbf{x}) = u(\mathbf{x}) - u_{\text{in}}(\mathbf{x}) = \int_{\Omega} g(\mathbf{x} - \mathbf{x}') f(\mathbf{x}') u(\mathbf{x}') d\mathbf{x}' \quad (5)$$

for any $\mathbf{x} \in \Gamma$. Note that the integrals (2) and (5) extend only over Ω because the scattering potential f is zero for all $\mathbf{x} \notin \Omega$.

The goal of inverse scattering is to estimate f , which is equivalent to ϵ , given M measurements of $\{u_{\text{sc}}(\mathbf{x}_m)\}_{m \in [1 \dots M]}$ in the sensor region Γ .

3.2 Iterative Born Approximation

At first glance, it might seem that (5) directly provides a linear relationship between f and u_{sc} , which can be used to solve the problem. However, the nonlinear nature of the inverse scattering becomes evident if one realizes that the internal field $u = u_{\text{in}} + u_{\text{sc}}$ in (5) depends on u_{sc} .

We now consider a K -term iterative Born approximation (IBA) [22] of the total field (2)

$$u_k(\mathbf{x}) = u_{\text{in}}(\mathbf{x}) + \int_{\Omega} g(\mathbf{x} - \mathbf{x}') f(\mathbf{x}') u_{k-1}(\mathbf{x}') d\mathbf{x}, \quad (6)$$

where $\mathbf{x} \in \Omega$, $u_0 = 0$, and $k = 1, 2, \dots, K$. When $K = 1$, eq. (6) reduces to the well-known first-Born approximation, which assumes a single scattering from f by approximating $u(\mathbf{x})$ with the incident field $u_{\text{in}}(\mathbf{x})$. For $K = 2$, the approximation of the total field is improved by taking into account the second scattering due to an additional interaction between the object and the field. For higher values of K the approximation is further improved by accounting for multiple scattering of order K (see also the discussion on multiple scattering by Born and Wolf [22]).

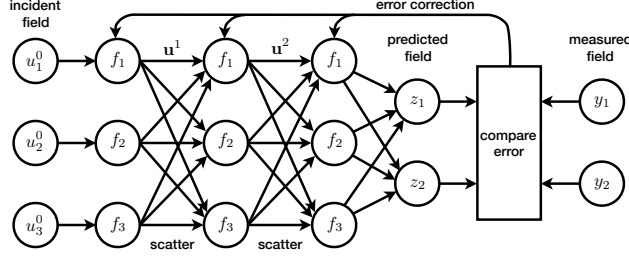


Figure 2: Schematic representation of the multiple scattering as a neural network for $K = 2$, $N = 3$, and $M = 2$. The scattering potential $\mathbf{f} \in \mathbb{R}^N$ plays the role of nonlinearities, while matrices $\mathbf{H} \in \mathbb{C}^{M \times N}$ and $\mathbf{G} \in \mathbb{C}^{N \times N}$ represent weights of the network. The error backpropagation algorithm described here allows to efficiently estimate \mathbf{f} by comparing predicted field $\mathbf{z} \in \mathbb{C}^M$ against the actual measurements $\mathbf{y} \in \mathbb{C}^M$.

In the context of general theory of integral equations, the iterations of type (6) are known as Liouville-Neumann series [23]. The sufficient condition for convergence states that the norm of the integral operator acting on the field should be less than unity. While this implies that IBA might diverge for large permittivity contrasts, it is still expected to work on a wide range of contrasts where the linearized models fail, which is corroborated by our simulations in Section 4.

3.3 Network Interpretation

We now discretize and combine equations (5) and (6) into the following matrix-vector recursion

$$\mathbf{z} \leftarrow \mathbf{H}(\mathbf{u}^K \odot \mathbf{f}), \quad (7a)$$

$$\mathbf{u}^k \leftarrow \mathbf{u}^0 + \mathbf{G}(\mathbf{u}^{k-1} \odot \mathbf{f}), \quad (7b)$$

for $k = 1, \dots, K$. Here, the vector $\mathbf{f} \in \mathbb{R}^N$ is the discretization of the scattering potential f , $\mathbf{z} \in \mathbb{C}^M$ is the predicted scattered field u_{sc} at sensor locations $\{\mathbf{x}_m\}_{m \in [1 \dots M]}$, $\mathbf{u}^0 \in \mathbb{C}^N$ is the discretization of the input field u_{in} inside Ω , $\mathbf{H} \in \mathbb{C}^{M \times N}$ is the discretization of the Green's function at sensor locations, $\mathbf{G} \in \mathbb{C}^{N \times N}$ is the discretization of the Green's function inside Ω , and \odot denotes a component-wise multiplication between two vectors. For every $k \in [1 \dots K]$, the vector $\mathbf{u}^k \in \mathbb{C}^N$ denotes the discretized version of the internal field after the k th scattering.

Figure 2 illustrates the representation of (7) as a feedforward neural network [24], where the edge weights are represented in \mathbf{H} and \mathbf{G} and the nonlinear nodes are described by the scattering potential \mathbf{f} . Note that the linear edge weights correspond to convolution operators and can thus be efficiently implemented with FFTs. Accordingly, the total computational cost of evaluating one forward pass through the network is $\mathcal{O}(KN \log(N))$.

3.4 Inverse Scattering

We formulate the inverse scattering as the following minimization problem

$$\hat{\mathbf{f}} = \arg \min_{\mathbf{f} \in \mathcal{F}} \{\mathcal{D}(\mathbf{f}) + \tau \mathcal{R}(\mathbf{f})\}, \quad (8)$$

where \mathcal{D} and \mathcal{R} are the data-fidelity and regularization terms, respectively, and $\tau > 0$ is the regularization parameter. The convex set $\mathcal{F} \subseteq \mathbb{R}^N$ enforces physical constraints on the scattering potential such as its, for example, non-negativity. The data-fidelity term is given by

$$\mathcal{D}(\mathbf{f}) \triangleq \frac{1}{2} \|\mathbf{y} - \mathbf{z}(\mathbf{f})\|_{\ell_2}^2,$$

where $\mathbf{y} \in \mathbb{C}^M$ contains measurements of the scattered field and \mathbf{z} is the field predicted by the recursion (7). As a regularization term, we propose to use isotropic TV penalty [25]

$$\mathcal{R}(\mathbf{f}) \triangleq \sum_{n=1}^N \|\mathbf{D}\mathbf{f}\|_{\ell_2} = \sum_{n=1}^N \sqrt{|\mathbf{D}_x\mathbf{f}|_n|^2 + |\mathbf{D}_y\mathbf{f}|_n|^2},$$

where $\mathbf{D} : \mathbb{R}^N \rightarrow \mathbb{R}^{N \times 2}$ is the discrete gradient operator with matrices \mathbf{D}_x and \mathbf{D}_y denoting the finite difference operations along x and y directions, respectively.

The optimization (8) can be performed iteratively using a proximal-gradient scheme or one of its accelerated variants [26–28]. Specifically, the scattering potential can be updated with the following iteration

$$\mathbf{f}^t \leftarrow \text{prox}_{\gamma\tau\mathcal{R}}(\mathbf{f}^{t-1} - \gamma\nabla\mathcal{D}(\mathbf{f}^{t-1})), \quad (9)$$

where $\gamma > 0$ is a step-size and

$$\text{prox}_{\tau\mathcal{R}}(\mathbf{g}) \triangleq \arg \min_{\mathbf{f} \in \mathcal{F}} \left\{ \frac{1}{2} \|\mathbf{f} - \mathbf{g}\|_{\ell_2}^2 + \tau\mathcal{R}(\mathbf{f}) \right\} \quad (10)$$

is the proximal operator, which corresponds to the TV regularized solution of the denoising problem. Note that, although, the proximal operator for isotropic TV does not admit a closed form, it can be efficiently computed [27]. The gradient $\nabla\mathcal{D}$ can be expressed as follows

$$\nabla\mathcal{D}(\mathbf{f}) = \text{Re} \left\{ \left[\frac{\partial}{\partial \mathbf{f}} \mathbf{z}(\mathbf{f}) \right]^H (\mathbf{z}(\mathbf{f}) - \mathbf{y}) \right\}, \quad (11)$$

where H is the Hermitian transpose of the Jacobian

$$\frac{\partial}{\partial \mathbf{f}} \mathbf{z}(\mathbf{f}) \triangleq \begin{bmatrix} \frac{\partial \mathbf{z}}{\partial f_1} & \cdots & \frac{\partial \mathbf{z}}{\partial f_N} \end{bmatrix}. \quad (12)$$

Then, by differentiating equations in (7) with respect to \mathbf{f} , and simplifying the resulting expressions, we obtain for any two vectors $\mathbf{r} \in \mathbb{C}^M$ and $\mathbf{b} \in \mathbb{C}^N$

$$\begin{aligned} \left[\frac{\partial \mathbf{z}}{\partial \mathbf{f}} \right]^H \mathbf{r} &= (\mathbf{H}^H \mathbf{r}) \odot \bar{\mathbf{u}}^K + \left[\frac{\partial \mathbf{u}^K}{\partial \mathbf{f}} \right]^H ((\mathbf{H}^H \mathbf{r}) \odot \mathbf{f}) \\ \left[\frac{\partial \mathbf{u}^k}{\partial \mathbf{f}} \right]^H \mathbf{b} &= (\mathbf{G}^H \mathbf{b}) \odot \bar{\mathbf{u}}^{k-1} + \left[\frac{\partial \mathbf{u}^{k-1}}{\partial \mathbf{f}} \right]^H ((\mathbf{G}^H \mathbf{b}) \odot \mathbf{f}), \end{aligned}$$

where $k = 1, \dots, K$, and vector $\bar{\mathbf{u}}$ contains complex conjugated elements of \mathbf{u} . These relationships lead to the following error backpropagation algorithm

$$\mathbf{g}^k \leftarrow \mathbf{g}^{k+1} + [\mathbf{G}^H \mathbf{v}^{k+1}] \odot \bar{\mathbf{u}}^k \quad (13a)$$

$$\mathbf{v}^k \leftarrow [\mathbf{G}^H \mathbf{v}^{k+1}] \odot \mathbf{f}, \quad (13b)$$

where $k = K - 1, K - 2, \dots, 0$, with the initialization $\mathbf{v}^K = [\mathbf{H}^H(\mathbf{z} - \mathbf{y})] \odot \mathbf{f}$ and $\mathbf{g}^K = [\mathbf{H}^H(\mathbf{z} - \mathbf{y})] \odot \bar{\mathbf{u}}^K$. The final value of the gradient (11) is obtained by returning $\nabla\mathcal{D}(\mathbf{f}) = \text{Re}\{\mathbf{g}^0\}$.

The remarkable feature of our error backpropagation approach is that it allows to efficiently evaluate the gradient of the scattered field with respect to the scattering potential. Due to the convolutional structure of the matrices, its computational complexity is equivalent to running a forward pass, which is of order $\mathcal{O}(KN \log(N))$. Equipped with this algorithm, the scattering potential can be optimized via iteration (9). Note that the algorithm does not explicitly evaluate and store the Jacobian (12) by instead computing its product with the residual $\mathbf{r} = (\mathbf{z}(\mathbf{f}) - \mathbf{y})$, as indicated in (11).

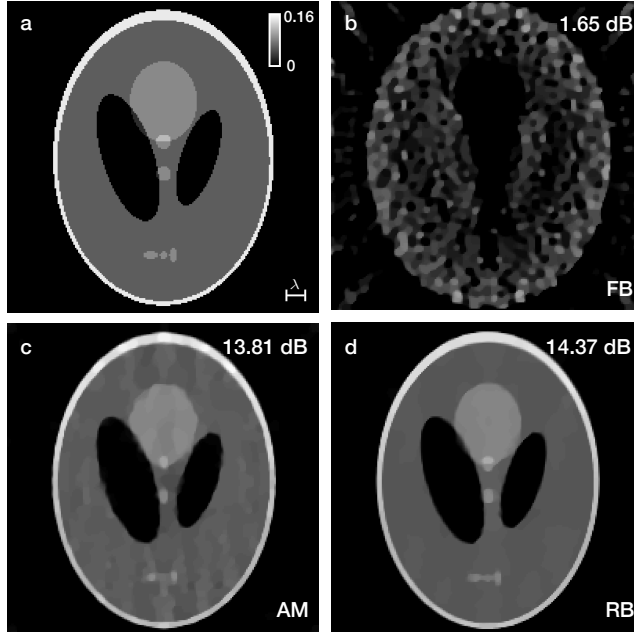


Figure 3: Evaluation on *Shepp-Logan* with 15% permittivity contrast at $\lambda = 7.49$ cm. (a) True contrast; (b) first-Born approximation; (c) alternating minimization; (d) proposed recursive-Born method with $K = 32$. Scale bar is equal to λ .

4 Experimental Validation

To validate our *Recursive Born (RB)* method, we report results for the tomographic experiment illustrated in Fig. 1, where the scattered wave measurements were obtained by running a high-fidelity Finite-Difference Time-Domain (FDTD) [29] simulator. The object is the *Shepp-Logan phantom* of size $82 \text{ cm} \times 112 \text{ cm}$ and the background medium is air with $\epsilon_b = 1$. The measurements are collected over 24 transmissions on a circle of radius $R = 100 \text{ cm}$ with 15° angle increments and, for each transmission, 360 measurements around the object are recorded. The dimensions of the computational domain for reconstruction are set to $L_x = L_y = 120 \text{ cm}$, with sampling steps $\delta x = \delta y = 0.6 \text{ cm}$, which implies a measurement ratio of $M/N \approx 22\%$. We define the *permittivity contrast* as $f_{\max} \triangleq (\epsilon_{\max} - \epsilon_b)/\epsilon_b$, where $\epsilon_{\max} \triangleq \max_{\mathbf{x} \in \Omega} \{\epsilon(\mathbf{x})\}$.

We compare results of our approach against two alternative methods. As the first reference method (denoted *first Born (FB)*), we consider the TV-regularized solution of linearized model based on the first-Born approximation, which is known to be valid only for weakly scattering objects. In addition to the linearized approach, we consider an optimization scheme (denoted *Alternating Minimization (AM)*) that alternates between updating the scattering potential for a fixed field and updating the field for a fixed scattering potential. This method is conceptually similar to the one proposed in [13], but with TV replacing the smooth regularizer, due to the edge-preserving properties of the former. Hence, all three methods minimize the same TV-regularized least-squares error functional; however, each method relies on a distinct physical forward model. Additionally, all the methods were initialized with zero, iterated until convergence by measuring the change in two successive estimates, and their regularization parameters were set to the same value $\tau = 10^{-9} \times \frac{1}{2} \|\mathbf{y}\|_{\ell_2}^2$.

Figure 3 compares the quality of the images obtained by all three methods for the permittivity contrast of 15% at $\lambda = 7.49 \text{ cm}$. Note that, due to the object's large size and contrast, FB fails to characterize its structure. Alternatively, both AM and RB succeed at recovering the object, with RB obtaining an image of significantly superior quality. Figure 4 illustrates the influence of the number of layers K on the quality of the reconstructed image (left), and the evolution of the relative data-fit $\|\mathbf{y} - \mathbf{z}\|_{\ell_2}^2 / \|\mathbf{y}\|_{\ell_2}^2$ for every iteration

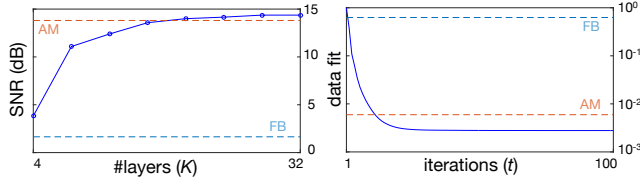


Figure 4: Illustration of the reconstruction performance on *Shepp-Logan* with 15% contrast. Left: SNR is plotted against the number of layers in the neural network. Right: normalized error between the true and predicted fields is plotted at each iteration for $K = 32$. Results obtained with FB and AM are marked with dashed lines.

Table 1: Comparison of three methods in terms of SNR for $\lambda = 10$ cm. The best result for each contrast is highlighted.

	Permittivity Contrast f_{\max}			
	5%	10%	15%	20%
First Born	9.20	5.40	2.98	1.58
Alternating Minimization	13.65	13.61	13.34	12.98
Recursive Born	14.86	14.07	13.71	13.65

with $K = 32$ (right). As can be appreciated from these plots, the proposed method outperforms FB and AM, both in terms of signal-to-noise ratio (SNR) and data-fit for networks with sufficient number of layers. Additionally, the method converges relatively fast—within first few tens of iterations.

Table 1 presents the results of quantitative evaluation of the methods for different values of the permittivity contrast at $\lambda = 10$ cm. As expected, the performance of all the methods degrades as the contrast value increases, which might be due to growing degree of nonlinearity, and hence, nonconvexity of the inverse scattering problem [30]. However, the solutions computed by the proposed RB approach are substantially better than the two alternatives, FB and AM, for all values of the contrast.

Finally, from a computational perspective, a single iteration of the method requires a number of FFTs proportional to the number of scattering layers. In our simulations, accurate results are obtained using about 100 iterations with networks of approximately 20 layers. More concretely, our basic MATLAB implementation requires about 1.3 seconds per iteration to process a transmission on a 4GHz Intel Core i7 processor with 32 GBs of memory.

5 Conclusion

The method developed in this paper reconstructs the distribution of the permittivity in an object from a set of measured scattered waves. In particular, the method accounts for multiple scattering of waves, in both transmission and reflection, and can thus be used when linearized models fail. The method is also computationally tractable due to its convolutional structure and can be further accelerated by parallelizing computations over multiple CPUs. We believe that the approach presented here opens rich perspectives for high-resolution tomographic imaging in a range of practical setups where multiple scattering is an issue.

References

- [1] A. C. Kak and M. Slaney, *Principles of Computerized Tomographic Imaging*. IEEE, 1988.
- [2] E. Wolf, “Three-dimensional structure determination of semi-transparent objects from holographic data,” *Opt. Commun.*, vol. 1, no. 4, pp. 153–156, September/October 1969.

- [3] A. J. Devaney, “Inverse-scattering theory within the Rytov approximation,” *Opt. Lett.*, vol. 6, no. 8, pp. 374–376, August 1981.
- [4] M. M. Bronstein, A. M. Bronstein, M. Zibulevsky, and H. Azhari, “Reconstruction in diffraction ultrasound tomography using nonuniform FFT,” *IEEE Trans. Med. Imag.*, vol. 21, no. 11, pp. 1395–1401, November 2002.
- [5] Y. Sung and R. R. Dasari, “Deterministic regularization of three-dimensional optical diffraction tomography,” *J. Opt. Soc. Am. A*, vol. 28, no. 8, pp. 1554–1561, August 2011.
- [6] T. Kim, R. Zhou, M. Mir, S. Babacan, P. Carney, L. Goddard, and G. Popescu, “White-light diffraction tomography of unlabelled live cells,” *Nat. Photonics*, vol. 8, pp. 256–263, March 2014.
- [7] F. Simonetti, “Multiple scattering: The key to unravel the subwavelength world from the far-field pattern of scattered wave,” *Phys. Rev. E: Stat., Nonlinear, Soft Matter Phys.*, vol. 73, no. 3, p. 036619, March 2006.
- [8] F. Simonetti, M. Fleming, and E. A. Marengo, “Illustration of the role of multiple scattering in sub-wavelength imaging from far-field measurements,” *J. Opt. Soc. Am. A*, vol. 25, no. 2, pp. 292–303, February 2008.
- [9] G. Maire, F. Drsek, J. Girard, H. Giovaninni, A. Talneau, D. Konan, K. Belkebir, P. C. Chaumet, and A. Sentenac, “Experimental demonstration of quantitative imaging beyond Abbe’s limit with optical diffraction tomography,” *Phys. Rev. Lett.*, vol. 102, p. 213905, May 2009.
- [10] U. S. Kamilov, I. N. Papadopoulos, M. H. Shoreh, A. Goy, C. Vonesch, M. Unser, and D. Psaltis, “Learning approach to optical tomography,” *Optica*, vol. 2, no. 6, pp. 517–522, June 2015.
- [11] P. M. van den Berg, *Scattering*. Academic Press, 2002, ch. Nonlinear Scalar Inverse Scattering: Algorithms and Applications, pp. 142–161.
- [12] A. G. Tijhuis, “Born-type reconstruction of material parameters of an inhomogeneous, lossy dielectric slab from reflected-field data,” *Wave Motion*, vol. 11, no. 2, pp. 151–173, May 1989.
- [13] Y. M. Wang and W. Chew, “An iterative solution of the two-dimensional electromagnetic inverse scattering problem,” *Int. J. Imag. Syst. Tech.*, vol. 1, pp. 100–108, 1989.
- [14] W. C. Chew and Y. M. Wang, “Reconstruction of two-dimensional permittivity distribution using the distorted Born iterative method,” *IEEE Trans. Med. Imag.*, vol. 9, no. 2, pp. 218–225, June 1990.
- [15] R. E. Kleinman and P. M. van den Berg, “A modified gradient method for two-dimensional problems in tomography,” *J. Comput. Appl. Math.*, vol. 42, no. 1, pp. 17–35, 1992.
- [16] —, “An extended range-modified gradient technique for profile inversion,” *Radio Sci.*, vol. 28, no. 5, pp. 877–884, September-October 1993.
- [17] K. Belkebir and A. Sentenac, “High-resolution optical diffraction microscopy,” *J. Opt. Soc. Am. A*, vol. 20, no. 7, pp. 1223–1229, July 2003.
- [18] P. M. van den Berg and R. E. Kleinman, “A contrast source inversion method,” *Inv. Probl.*, vol. 13, no. 6, pp. 1607–1620, December 1997.
- [19] L. Tian and L. Waller, “3D intensity and phase imaging from light field measurements in an LED array microscope,” *Optica*, vol. 2, pp. 104–111, 2015.
- [20] L. Waller and L. Tian, “Machine learning for 3D microscopy,” *Nature*, vol. 523, no. 7561, pp. 416–417, July 2015.

- [21] U. S. Kamilov, I. N. Papadopoulos, M. H. Shoreh, A. Goy, C. Vonesch, M. Unser, and D. Psaltis, “Optical tomographic image reconstruction based on beam propagation and sparse regularization,” *IEEE Trans. Comp. Imag.*, vol. 2, no. 1, pp. 59–70, March 2016.
- [22] M. Born and E. Wolf, *Principles of Optics*, 7th ed. Cambridge Univ. Press, 2003, ch. Scattering from inhomogeneous media, pp. 695–734.
- [23] G. B. Arfken and H. J. Weber, *Mathematical Methods for Physicists*, 6th ed. Elsevier, 2005, ch. Integral equations, pp. 1005–1036.
- [24] C. M. Bishop, *Neural Networks for Pattern Recognition*. Oxford, 1995.
- [25] L. I. Rudin, S. Osher, and E. Fatemi, “Nonlinear total variation based noise removal algorithms,” *Physica D*, vol. 60, no. 1–4, pp. 259–268, November 1992.
- [26] J. M. Bioucas-Dias and M. A. T. Figueiredo, “A new TwIST: Two-step iterative shrinkage/thresholding algorithms for image restoration,” *IEEE Trans. Image Process.*, vol. 16, no. 12, pp. 2992–3004, December 2007.
- [27] A. Beck and M. Teboulle, “Fast gradient-based algorithm for constrained total variation image denoising and deblurring problems,” *IEEE Trans. Image Process.*, vol. 18, no. 11, pp. 2419–2434, November 2009.
- [28] U. S. Kamilov, “Parallel proximal methods for total variation minimization,” in *IEEE Int. Conf. Acoustics, Speech and Signal Process. (ICASSP 2016)*, Shanghai, China, March 19-25, 2015, arXiv:1510.00466 [cs.IT].
- [29] A. Taflove and S. C. Hagness, *Computational Electrodynamics: The Finite-Difference Time-Domain Method*, 3rd ed. Artech House Publishers, 2005.
- [30] O. M. Bucci, L. Cardace, L. Crocco, and T. Isernia, “Degree of nonlinearity and a new solution procedure in scalar two-dimensional inverse scattering problems,” *J. Opt. Soc. Am. A*, vol. 18, no. 8, pp. 1832–1843, August 2001.